



Marshall Plan Scholarship Program

*in collaboration between*

*Soft Electronics Laboratory (SEL) of Johannes Kepler University, Linz, Austria*

*And*

*Atwater Research Group of California Institute of Technology, Pasadena, CA, USA*

# Ultralightweight Perovskite Solar Cells for Outer Space Applications

Submitted as a project report

*In fulfilment of the Terms of the Marshall Plan Scholarship*

*by*

*Stepan Demchyshyn*

February 2020

## Acknowledgment

I would like to thank Prof. Martin Kaltenbrunner for supporting this work both practically and intellectually, as well as Prof. Harry Atwater for granting me an opportunity to work in his laboratory and his continuous support of this collaboration. Especially I would like to express my gratitude to Dr. Michael Kelzenberg for his guidance, being a great teacher and a good friend throughout the time of the research visit.

Additionally, I would like to thank perovskite and space solar power team members at California Institute of Technology, namely Samuel Loke, Arky Yang, Nina Vaidya, Jonathan Grandidier, Pilar Espinet, Kyle Virgil and everybody else at the Atwater Research group. I am also very grateful to my colleagues and collaborators from Soft Electronics Laboratory and Linz Institute of Organic Solar Cells at Johannes Kepler University for their help and support, specifically Bekele Heiligenaw, Matteo Verdi, Lukas Lehner, Stephan Schaumüller, Doris Cristurean, Markus Scharber, and Serdar Sariciftci. I am also very thankful to administrative assistant Kam Flower at California Institute of Technology and Christa Mitschan at Johannes Kepler University for their invaluable support in day-to-day and procedural matters.

Also I would like to acknowledge financial support from Marshal Plan Foundation that made this research visit possible and European Research Council that funds my doctoral research.

## Abstract

Creating an efficient, lightweight, and sustainable source of power for space exploration is one of the main challenges of aerospace community that has been often addressed using photovoltaic technology. While state-of-the-practice photovoltaic technology is already supporting missions as distant as Juno that is currently orbiting Jupiter, its high mass and susceptibility to radiation damage imposes limits on the ultimate performance and lifetime. Perovskite solar cells have recently emerged as one of the most rapidly advancing thin film solar cell technologies showing high performance and radiation hardness. Hence, ultra lightweight perovskite solar cells fabricated on micrometer-thin polymer substrate previously developed in our lab are promising candidates for space application. During this research visit, performance of ultra lightweight perovskite solar cells was examined under low temperature, high temperature, and low intensity – low temperature conditions, as well as under simulated low Earth orbit environment. Two perovskite compositions were examined with mixed cation mixed anion emerging as the more stable and reliable. Framework was established for practical aspects of ultra lightweight perovskite solar cell form factor measurements that will allow for future collaboration between Johannes Kepler University and California Institute of Technology.

# Contents

Acknowledgment .....	2
Abstract .....	3
Contents .....	4
Introduction .....	5
Perovskites .....	5
Flexible electronics and perovskite solar cells .....	7
Solar cells on spacecrafts .....	8
Space environment and perovskite solar cells .....	9
Methods .....	12
Materials .....	12
Solution preparation .....	12
Device fabrication .....	13
Characterization .....	15
Measurement set-up .....	15
Results .....	16
Mixed anion perovskite solar cells temperature cycling .....	16
Mixed cation mixed anion solar cells low intensity – low light testing .....	22
Mixed cation mixed anion solar cell low Earth orbit simulation .....	24
Conclusions and Outlook .....	27
Bibliography .....	29

## Introduction

### Perovskites

Metal halide perovskite has achieved the quickest and most impressive progress amongst all photovoltaic materials. The name perovskite originally referred to a crystal structure of calcium titanium oxide ( $\text{CaTiO}_3$ ) [1]. This mineral was first discovered by a 19<sup>th</sup> century Prussian mineralogist Gustav Rose in a piece of chlorite-rich skarn and named after Russian nobleman and mineralogist Lev Alekseevich von Perovski on suggestion of famous mineral collector August Alexander Kammerer [2]. Later, it has been discovered that a number of other minerals ( $\text{BaTiO}_3$ ,  $\text{PbTiO}_3$ ,  $\text{SrTiO}_3$ , *etc.*) have this crystal structure too, giving the name a broader definition. Nowadays, the name perovskite refers to a family of compounds that have an empirical formula of  $\text{ABX}_3$  where an idealized cubic unit cell having A atom at cube corner positions (0, 0, 0), B atom sitting in body center positions ( $\frac{1}{2}$ ,  $\frac{1}{2}$ ,  $\frac{1}{2}$ ), and X atoms at face center positions ( $\frac{1}{2}$ , 0, 0; 0,  $\frac{1}{2}$ , 0; 0, 0,  $\frac{1}{2}$ ) (Fig. 1a) [3]. Most of the naturally occurring perovskites can be found in the lower Earth mantle, including compounds like bridgmanite or knopite [2]. Initially, the interest in this materials family arose due to high temperature super conductivity discovered in copper - based oxide perovskite [4]. This followed by research in related fields finding application for perovskites in capacitors [5], piezoelectric devices [6], scintillators [7], catalysis [8], colossal magnetoresistance research [9], ferroelectrics [10], and multiferroics [11]. One of the first investigation of metal halide perovskites was done on  $\text{CsPbBr}_3$  in 1893 by Wels *et al.* [12], but its actual structure was identified only years later in 1958 by C. K. Moller [13]. In 1978, Weber has discovered that  $\text{Cs}^+$  can be easily replaced by organic methylammonium cation ( $\text{CH}_3\text{NH}_3^+$ ) and was the first to report on organic inorganic metal halide perovskites [14]. Nevertheless, the seminal work of Miyasaka and colleagues in 2009 [15] followed by the work of Snaith and colleagues in 2012 [16] were the first to recognize  $\text{CH}_3\text{NH}_3\text{PbI}_3$  as an auspicious photovoltaic active material. Their publications have catalyzed an avalanche of research and kickstarted successful field of study with most recent devices showing certified 23.7 % power conversion efficiency [1]. The unique crystalline structure, that gives rise to an unmatched success of this material, can be maintained only in combination of certain atomic radii of its constituent components. The relationship between each individual atom is controlled by an empirical Goldschmidt tolerance factor ( $\alpha$ ) and is defined as follows:

$$\alpha = \frac{r_A + r_B}{\sqrt{2}(r_A + r_X)} \quad (1)$$

where  $r_A$  – atomic radius of a cation,  $r_B$  – atomic radius of a metal center, and  $r_X$  – atomic radius of an anion. The Goldschmidt equation suggests that the perovskite structure will be preserved only

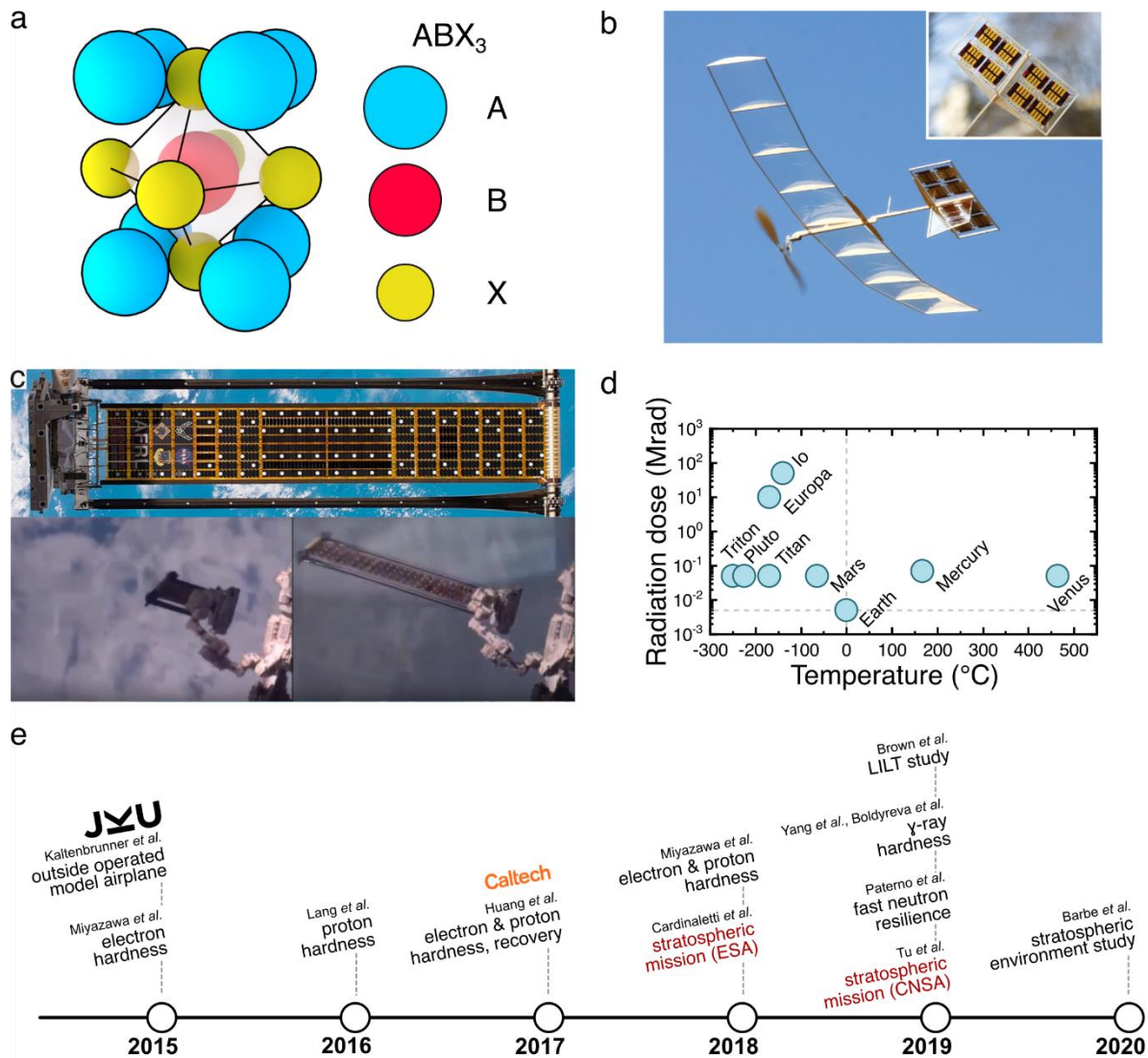


**Figure 1. Flexible photovoltaics for aerospace application. (a)** Perovskite crystal structure, with an empirical formula  $ABX_3$ , where A (blue) refers to cation, B (red) refers to metal center, and X (yellow) refers to halide anion. **(b)** Solar-powered model airplane utilizing ultra lightweight perovskite photovoltaics fabricated on  $1.4 \mu\text{m}$  operating in outdoor conditions [17]. **(c)** Images of Roll-Out Solar Array (ROSA) from International Space Station (ISS), operating between April and September 2017, demonstrating compact deployable photovoltaic structure. Highlighted are pictures of ROSA fully unrolled (top), at the beginning (bottom left), and at the end of deployment (bottom right) [18], [19]. **(d)** Outline of extreme environmental challenges (high radiation and low/high temperatures) facing spacecrafts around selected bodies in our solar system [20]. **(e)** Timeline of selected recent publications that consider perovskite solar cells for space application by examining their radiation hardness, simulating performance under low intensity - low temperature conditions, as well as reporting on high - altitude stratospheric mission results of these photovoltaic technology.

if  $\alpha \approx 0.8 - 1$  [21]. In current state-of-the-art formulations of metal halide perovskites for solar cells, A-site is occupied by methylammonium, formamidinium, and Cs, B-site is a metal center containing Pb or Sn, and X-site is populated by a halide anion [1]. Additionally, metal halide perovskites distinctive ionic crystal nature allows it to compete well with conventional covalent semiconductors. Ease of processing using solution techniques and its high absorption coefficient allows it to be used as a thin film. Unparalleled defect tolerance that results in large carrier diffusion length and suppressed recombination together with broad absorption spectrum contribute to superior performance and high efficiency of perovskite based solar cells [1]. Over time, metal halide perovskites have found application not only in photovoltaics, but also in optoelectronics [22], radiation sensors [23], and information storage technology [24].

### Flexible electronics and perovskite solar cells

Fabricating electronics on flexible substrates dates back to middle of the last century when curiosity driven scientists at Westinghouse Laboratory fabricated first flexible logic in 1967 [25]. In the same year, K. A. Ray of Hughes Aircraft Company reported first Si solar cell on flexible foil and its related space deployable structure, stating that the first discussion of this idea took place as early as 1958 [26]. The next major step in flexible electronics took place in 1999 when amorphous Si thin-film transistor was fabricated on 3  $\mu\text{m}$  steel substrate allowing for the pioneerign demonstration of ultrathin and ultraflexible device [27]. Renewed interest in these types of devices was sparked by the development of imperceptible organic electronics [28]. Fabricating thin-film electronic layers in the neutral mechanical plane between substrate and encapsulation structure allowed for extreme mechanical behavior and minute bending radii. Examples of devices fabricated on 1.4  $\mu\text{m}$  foil usually used for capacitors include active-matrix array sensors, thin-film transistors, and light emitting diodes (LEDs) [29], [30]. This was followed by first demonstration of organic and then perovskite solar cells in this form factor [17], [31]. Kaltenbrunner *et al.* have fabricated ultra lightweight perovskite solar cells on 1.4  $\mu\text{m}$  PET foil, resulting in the total device thickness of about 3  $\mu\text{m}$  and record-breaking power-per-weight ratio of 23  $\text{W g}^{-1}$ . As predicted, these solar cells also showed unprecedented resilience to mechanical deformation and bending radii that could be reduced to 10  $\mu\text{m}$ . The results were demonstrated by operating a small model glider airplane using a small array of these devices (Fig. 1b).

Flexible and ultra lightweight solar cells extend the realm of photovoltaics application beyond that what is possible with hard, planar, and bulky conventional solar cells. Potential applications range from wearable electronics [32], electronic textiles [33], artificial skin [34], and application on deformable surfaces that can be extended though medical, safety, security, infrastructure, and communication

industries [35]. Specific advantage of perovskite solar cells is its high conversion efficiency in low light conditions that is especially relevant for wearable devices [36]. Furthermore, production of flexible photovoltaics can be done via roll-to-roll process that can significantly decrease its cost and make production time considerably smaller, as it has been shown in examples of organic solar cells [37] and dye sensitized solar cells [38]. While many of the previous generation photovoltaic technologies that have been dominating the market, like amorphous Si [39], GaAs [40], CdTe [41], and CIGS [42], have already been made flexible, low cost and ease of production position perovskites as a worthy competitor in the field of flexible solar cells. On the whole, the ultra lightweight perovskite solar cells possess a number of properties like high efficiency, small thickness, and extreme bendability that is useful for transportation and storage while also reducing additional cost related to fabrication and installation.

### Solar cells on spacecrafts

Aerospace is a field where inherent properties of ultra lightweight solar cells like high specific power, low area density, and low stowage volume are of outmost importance. Historically, space application has been the major driver for the development of photovoltaic solar panels [43]. First solar powered satellite was Vanguard 1 launched in 1958 that had just eight  $2 \times 0.4$  cm silicon cells connected in series attached to its body [44]. These cells provided only 50 mW of power and had about 8 % power conversion efficiency. Vanguard 1 transmitted signal for almost 6 years using these solar cells, as opposed to its battery powered contender Sputnik 1 that worked only for three weeks [43]. Solar cells remain the standard space application energy source. Photovoltaics in outer space power a range of sensors, assist with thermal control, telemetry as well as power propulsion systems [43], [45]. Some more recent mission examples including Magellan that was used to map out the surface of Venus, Mars Global Surveyor that helped to pave the way for Mars rovers, or Hubble that is the first space telescope [45]. One of the most impressive examples of solar powered spacecrafts is Juno that currently orbits in the extreme environment of Jupiter. Its three 9 m arrays containing 18,698 single cells operate in low intensity – low temperature conditions and additionally designed to withstand severe radiation surrounding the largest planet in our solar system [46], [47].

While gallium arsenide-based multijunction solar cells are state-of-the-practice technology at the moment, perovskite photovoltaics have also been theorized to become useful sources of energy for future space mission. Examples include high altitude pseudo satellites (HASP) [48], operation under low intensity – low temperature conditions in outskirts of our solar systems [49], and endeavoring projects like Space-Based Solar Power [50]. Practically, these applications will require integration with advanced deployable

structures which will benefit from ultra lightweight form factor. Existing designs and prototypes include retractable solar array “blankets” on International Space Station (ISS) [51], experimental Roll Out Space Array (ROSA) that was unfurled and tested in Earth orbit in 2017 (Fig. 1c) [52], or even more complex lightweight coilable ladder-type structure proposed by Gdoutos *et al.* [53]. While large solar arrays are setting excellent examples of what can be achieved with solar power in space, there exists a burgeoning field of small spacecrafts that include mini- (ca. 100 kg), micro- (10-100 kg), nano- (1-10 kg) or even pico- (0.01-1 kg) and femtosatellites (0.001-0.01 kg) that also require solar power (85 % of small spacecrafts are powered via solar cells) [54]. This research and technology aims to not only incrementally improve the existing capabilities but bring forward new and revolutionary approaches which would otherwise take too long to develop on larger structures. Combination of ultra lightweight perovskite solar cells’ intrinsic high flexibility and body of deployable structure knowledge makes perovskite photovoltaics a great candidate for aerospace applications.

### Space environment and perovskite solar cells

While devoid of moisture and oxygen, the main factors contributing to perovskite solar cell degradation on Earth, harsh environment of outer space still presents a plethora of scientific and engineering challenges for any photovoltaic technology. Past, current, and future missions orbiting Earth, performing fly - byes or orbiting other planets in our solar system must face both extremely low and high temperatures, as well as withstand severe levels of radiation (Fig. 1d) [20]. Temperature profiles are dependent on the distance from the Sun as well as on the amount of heat produced by a space body. Systems on board of spacecraft to Venus might have to withstand temperatures as high as 460 °C, while missions to Neptune will need to survive -200°C [55]. The Sun, besides being the source of light, is also the source of solar wind which fills the vast empty space in our solar system with considerable amounts of radiation. Solar wind is mostly a stream of protons and electrons moving past Earth with an average speed of 400-500 km/h. In addition to solar wind, the Sun tends to have flares, sunspots, prominence, spicules, plages, and facula over time. Another source of radiation is galactic cosmic rays consisting of mostly protons, but also alpha particles and heavy nuclei coming from beyond our solar system. Both types of radiation coming from the Sun and outside of our solar system can be trapped in a planetary magnetic field to create unique radiation environments. While some planets like Mars and Venus have no or very weak magnetic fields, others like Jupiter, Neptune or Uranus have extremely strong magnetic fields creating permanent radiation belts. Earth with 0.3 G of magnetic field has a region of trapped particles called the Van Allen belts that present a significant issue for spacecrafts travelling through it or satellites operating in its vicinity [43], [45]. Further difference in space for photovoltaics lies in solar spectrum that

is unfiltered by Earth atmosphere. It is referred to as Air Mass Zero (AM0), as opposed to Air Mass 1.5 (AM1.5) on Earth, and has to be considered when testing solar cells for aerospace application. Despite solar intensity being higher in space, solar cells often perform worse under AM0 due to difference in spectral distribution.

While some knowledge of perovskite solar cells behavior under low or high temperatures is available, an increasing number of studies over the last five years have focused on perovskites as potential active material for space application (Fig. 1e). A study by Miyazawa *et al.* [56] has noted perovskite's hardness to electron irradiation as early as 2015 ( $E = 1 \text{ MeV}$ , rate =  $1 \times 10^{12} \text{ cm}^{-2}\text{s}^{-1}$ ,  $H_e = 1 \times 10^6 \text{ cm}^{-2}$ ), which then was followed by several studies by this and other groups including both electron and proton ( $E = 50 \text{ keV}$ , rate =  $3 \times 10^{11} \text{ cm}^{-2}\text{s}^{-1}$ ,  $H_e = 1 \times 10^{12}$  to  $1 \times 10^{15} \text{ cm}^{-2}$ ) hardness [57]–[62]. Work by Yang *et al.* [63] and Boldyreva *et al.* [64] report different outcomes for stability of perovskite after gamma ray irradiation. Yang *et al.* report perovskite solar cells to retain 97 % of their efficiency after irradiation with accumulated dose of 2.3 Mrad. On the other hand, Boldyreva *et al.* report degradation of solar cells (25-35 % of its initial value) after material absorbing only 0.05 Mrad of gamma ray radiation. This suggests that additional studies must be conducted, that will take into account specific perovskite composition and device architecture. Paterno *et al.* investigated perovskite solar cell performance before and after fast neutron ( $>10 \text{ MeV}$ ) irradiation, reporting high resilience to this type of severe form of radiation [65]. A high-altitude balloon OSCAR (Optical Sensors based on CARbon materials) mission as a part of REXUS/BEXUS (Rocket and Balloon Experiments for University Students) program by European Space Agency was the first to have perovskite solar cells ( $\text{CH}_3\text{NH}_3\text{PbI}_3$ ) operating for about 3 h in stratospheric conditions (about 30 km altitude) and reported significant drop of power conversion efficiency from initial 14 to 9 % after the flight [66]. A similar mission conducted by researchers from China reports a rigid perovskite solar cell sample ( $\text{FA}_{0.81}\text{MA}_{0.10}\text{-Cs}_{0.04}\text{PbI}_{2.55}\text{Br}_{0.40}$ ) returning back from 2 h stratospheric flight (35 km altitude) retaining about 95 % of its original power conversion efficiency [67]. Moreover, Brown *et al.* showed good performance of rigid perovskite solar cells [ $(\text{FA}_{0.79}\text{MA}_{0.16}\text{Cs}_{0.05})_{0.97}\text{Pb}(\text{I}_{0.84}\text{Br}_{0.16})_{2.97}$ ] in simulated low intensity – low temperature environments common for outer planetary missions to places like Jupiter, Saturn, and their moons [49]. Their study suggests that perovskite solar cells can perform well under these conditions maintaining high power conversion efficiency and having lower hysteresis. As recently as 2020 a study was also published by Barbe *et al.* reporting compatibility and reliable performance (80 % PCE after 25 days of day - night cycles) of mixed cation -mixed anion perovskite rigid solar cells [ $\text{Cs}_{0.05}(\text{MA}_{0.17}\text{FA}_{0.83})_{0.95}\text{Pb}(\text{I}_{0.83}\text{Br}_{0.17})_3$ ] under low pressure low temperature simulated stratospheric

conditions (-70 to 20 °C, 10 mbar), giving even stronger support to perovskite solar cell application in aerospace [48].

## Methods

### Materials

All chemicals and solvents were purchased from commercial suppliers and used as received, if not stated otherwise. The list of materials used during this project include Hellmanex III detergent (Hellma Analytics), Sylgard 184 Silicone Elastomer (PDMS, Dow Corning), polyethylene terephthalate foil (PET, Mylar® CW02), n-hexane (VWR, 98 %), PEDOT-PSS aqueous dispersion (Clevios PH1000, Heraeus), Zonyl FS-300 (abcr GmbH), lead chloride (PbCl<sub>2</sub>, Sigma Aldrich, 98 %), lead iodide (PbI<sub>2</sub>, Sigma Aldrich, 99.9 %), lead bromide (PbBr<sub>2</sub>, Sigma Aldrich, 99.99 %), cesium iodide (CsI, Sigma Aldrich, 99.9 %), N,N-dimethylformamide (DMF, anhydrous, Sigma Aldrich), dimethylsulfoxide (DMSO, VWR, 99.5 %), acetyl acetone (AA, CH<sub>3</sub>COCH<sub>2</sub>COCH<sub>3</sub>, Sigma-Aldrich, ≥99 %), chlorobenzene (VWR, reagent grade), N,N'-dimethyl-3,4,9,10-perylenetetracarboxylic diimide (PTCDI, purified through sublimation 2 times, Hoechst), epoxy (EPO5.S200, Conrad.at), 4,4'-biphtalic anhydride (dianhydride, CAS RN:2420-87-3, TCI Chemicals), 9,9-bis(4-aminophenyl)fluorene (diamine, CAS RN:15499-84-0, TCI Chemicals), and 1-methyl-2-pyrrolidinone (NMP, anhydrous, 99.5 %, Sigma Aldrich).

Methylammonium bromide (MABr) was synthesized from methylamine (33 wt% in absolute ethanol; Sigma Aldrich) and hydrobromic acid (HBr, 48 wt%, aqueous; Sigma Aldrich) and purified using diethylether (VWR) and absolute ethanol (Merck Millipore) as described in literature [68], [69]. Methylammonium iodide (MAI) and formamidinium iodide (FAI) were synthesized using analogous procedure using hydroiodic acid (HI, 57 wt%, aqueous; Sigma Aldrich).

Polyimide (PI) was synthesized using procedure reported by Hulubei *et al.* [70]: dianhydride (0.588 g, 2 mmol) was added under continuous stirring over diamine (0.696 g, 2 mmol) that was dissolved in 6.5 mL anhydrous NMP in three-necked round bottom flask fitted with N<sub>2</sub> inlet and outlet tube, mechanical stirrer and a reflux condenser. The reaction was stirred at room temperature over night to yield polyamic acid (PAA). Polyimide films were prepared by spin coating (1700 rpm, 30 s) PAA precursor (20 wt% in NMP) onto glass slides that was then annealed at 185 °C for 1 hour under ambient conditions.

### Solution preparation

PDMS solution was prepared by mixing 1:10 w/w of crosslinker to hardener and then diluting it 1:2 w/w with hexane.

PEDOT solution was prepared by mixing Clevis PH1000 stock solution with 5 vol% DMSO and 0.5 % Zonyl FS-300, stirring at room temperature for an hour and keeping at 4 °C overnight. PEDOT solution was filtered through Minisart RC25 Syringe filter 0.45 µm regenerated cellulose right before use.

Mixed anion perovskite precursor solution ( $\text{CH}_3\text{NH}_3\text{Pb}_{1-x}\text{Cl}_x$ ) was prepared according to procedure reported in Heiligenaw *et al.* [71].  $\text{PbCl}_2$  (144.5 mg, 0.5 mmol),  $\text{PbI}_2$  (239.6 mg, 0.5 mmol) and  $\text{CH}_3\text{NH}_3\text{I}$  (256.0 mg, 2.3 mmol) were dissolved in 1 mL of DMF and AA (9:1 v/v ratio respectively) followed by stirring at 45 °C overnight. The solution was passed through polytetrafluoroethylene syringe filters (0.45 µm; Whatman) before spin coating.

Mixed cation - mixed anion perovskites [ $\text{Cs}_{0.05}(\text{FA}_{0.83}\text{MA}_{0.17})_{0.95}\text{Pb}_{1-x}\text{Br}_x$ ] precursor solution was prepared according to procedure reported in Heiligenaw *et al.* [72].  $\text{PbI}_2$  (507.5 mg, 1.10 mmol), FAI (172 mg, 1.00 mmol), MABr (22.4 mg, 0.20 mmol), and  $\text{PbBr}_2$  (73.5 mg, 0.20 mmol) were mixed in 1 mL of DMF and DMSO (4:1 v/v ratio respectively) followed by stirring at 45 °C until dissolved. Afterwards, CsI (*ca.* 0.063 mmol, from 1.5 M stock solution in DMSO) was added to the mixture and stirred overnight. Parent solution was passed through polytetrafluoroethylene syringe filters (0.45 µm; Whatman) before spin coating.

### Device fabrication

Glass substrates (2.5 × 2.5 cm, 1 mm thick) were cut and cleaned in an ultrasonic bath for 30 min each in 2 v/v% Hellmanex in DI water solution, 2×DI water solution, isopropanol and dried using  $\text{N}_2$ . Then PDMS solution was spin coated at 4000 rpm for 30 s on glass and placed on a heat plate at 150 °C for 10 min to cross-link. Next, the 1.4 µm PET foil was carefully placed on the sample avoiding air pockets and then transferred to a heating plate again at 110 °C for another 10 min. Afterwards, Cr/Au (10/100 nm) busbars were thermally evaporated (0.1-1 nm  $\text{s}^{-1}$  at base pressure  $\sim 1 \times 10^{-6}$  mbar). Highly conductive PEDOT solution was spin coated 1500 rpm for 45 s (ramp 2 s) followed by 1000 rpm for 2 s (ramp 1 s) and annealed at 122 °C for 15 min. Then the film was washed by spin-coating isopropanol solution at 1500 rpm for 4 s followed by 4000 rpm for 12 s and annealed at 120 °C for 15 min.

Mixed anion perovskite precursor solution was spin coated under ambient conditions at 1300 rpm (ramp 2 s) for 17 s followed by 2000 rpm (ramp 2 s) for 5 s. Then the films were annealed at 115 °C for 40 min.

Mixed cation - mixed anion perovskites films were processed inside  $\text{N}_2$  glovebox. Precursor solution was deposited using anti-solvent procedure. First the solution was spin-coated at 1500 rpm for 10 s (ramp 9 s) followed by 6000 rpm for 30 s (ramp 2 s). *Ca.* 0.2 mL of chlorobenzene (anti-solvent) was dropped at 23<sup>rd</sup>

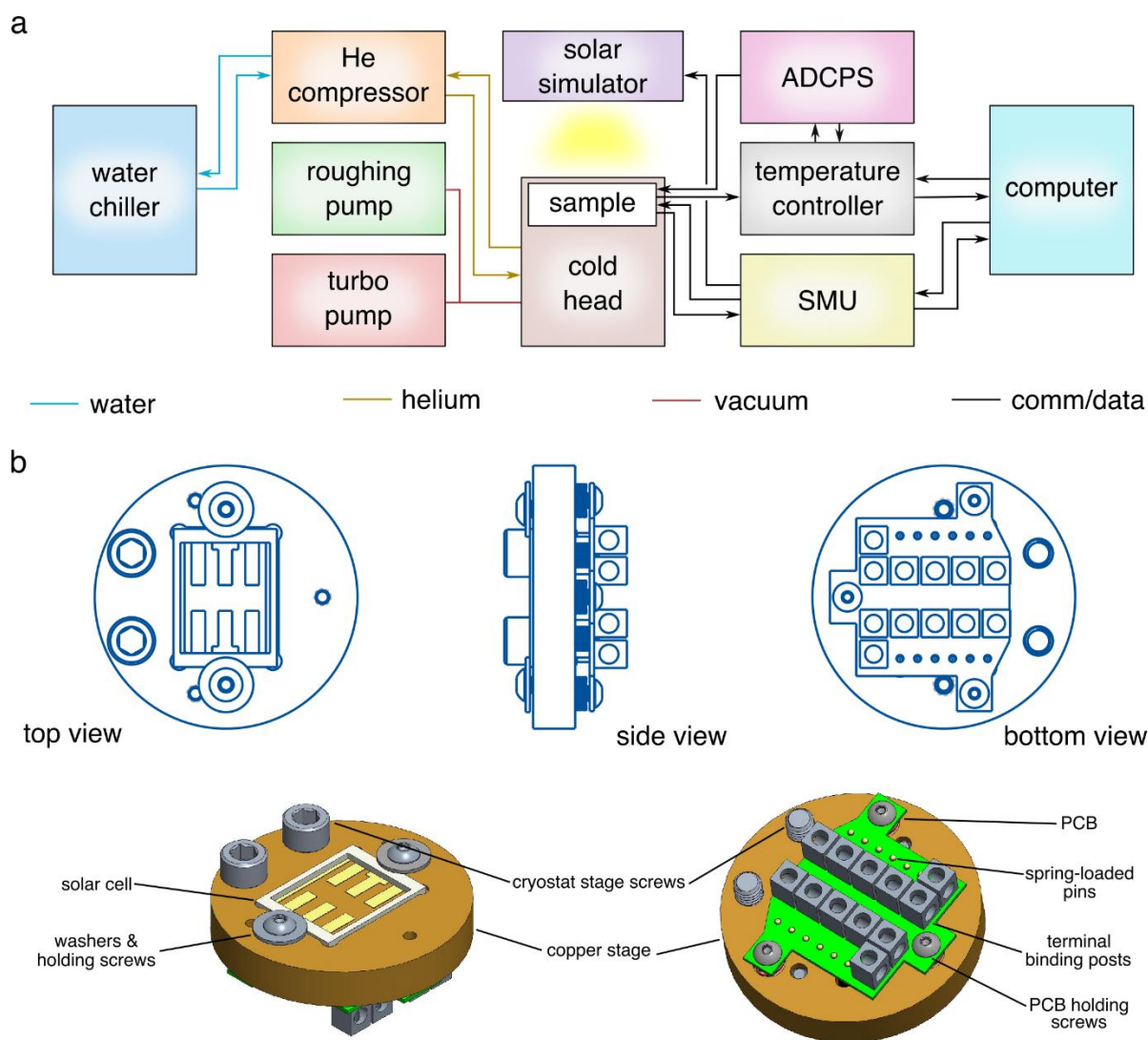


**Figure 2. Experimental set-up and sample holder. (a)** Block diagram of the experimental set-up built for vacuum thermal cycling experiment. Cold head that houses the sample is connected to a He compressor and high vacuum pump system in order to allow low - temperature high - vacuum measurements. Temperature can be raised via a resistive heating element connected to an adjustable DC power source (ADCPS) and controlled through temperature controller. Source Measurement Unit (SMU) is used to perform electrical measurement (JV sweeps, maximum power point tracking, etc.) and open/close shutter in front of the solar simulator. SMU and temperature controller are operated using in - lab written software in Python. **(b)** Assembly drawing of a custom - built cryostat sample holder for a flexible solar cell on a plastic frame support, highlighting its copper body, custom designed printed circuit board and terminal posts for electrical contact.

second for about 3 s. Then the film was annealed at 100 °C for 1 h. 150 nm PTCDI layer was deposited via thermal evaporation at 0.5-2 nm s<sup>-1</sup> rate and base pressure  $\sim 1 \times 10^{-6}$  mbar. This was followed by thermal evaporation of Cr/Au contacts (10/100 nm) at rate of 0.1-1 nm s<sup>-1</sup> and base pressure  $\sim 1 \times 10^{-6}$  mbar. 1.5 μm thin PI film was used for encapsulation and mechanical reinforcement. A layer of epoxy was spin coated (2000 rpm, 30 s) onto the PI film and then it was promptly lifted off the glass and transferred onto the solar cell, epoxy layer facing towards the solar cell. Flexible solar cells were lifted from their glass support using transfer printing technique with Parafilm as the carrier in order to provide additional mechanical support and reduce bending stress during transfer. Resulting solar cells (6 pixels on every device, 0.11 cm<sup>2</sup> each) were fixed to a plastic PET frame using double sided Kapton tape allowing to handle them in their freestanding form.

### Characterization

Electrical characterization at JKU were performed using Keithley 2400 Source Measurement Unit. JV sweeps were performed at 200 mV/s rate inside of a N<sub>2</sub> glovebox under AM1.5 illumination. Samples were transferred between the labs inside of sealed aluminum coated Mylar bags filled with N<sub>2</sub> and later stored inside N<sub>2</sub> box. JV measurements at Caltech were performed using Keithley 2400 Source Measurement Unit under ambient conditions at 200 mV/s unless stated otherwise. Maximum Power Point Tracking measurement was adapted from Rakocevic *et al.* [73].  $V_{MPP}$  and  $J_{MPP}$  were determined from a single IV sweep, Perturb and Observe algorithm was used with  $n$  (number of measurements) = 5,  $\Delta V$  (voltage step size) = 50 mV,  $d$  = 3 s.

### Measurement set-up

Cryostat measurement set-up that was built in the course of this research visit is shown in Fig. 2a. It allows for measurements in high vacuum conditions, cooling via He compressor, controlling temperature via Adjustable DC Power Source (ADCPS) and temperature controller, performing electrical measurements and controlling the solar simulator via Source Measurement Unit (SMU) Keithley 2400. Sample was placed in the cold head of the cryostat and thermally contacted using thermally conducting grease (Apiezon N Cryogenic High Vacuum Grease from SPI Supplies) and electrical measurements were done using custom build sample holder consisting of copper body, PCB, and spring-loaded pins for to contact individual pixels (Fig. 2b). Hardware was addressed and the data was collected using custom written Python software.

## Results

### Mixed anion perovskite solar cells temperature cycling

Initial low temperature testing was performed on mixed anion perovskite solar cells (Fig. 3a) under high vacuum conditions and AM1.5 illumination with a dual purpose of accessing set-up working parameters and testing mixed anion perovskite solar cell performance. After storage and transportation between the labs (Fig. 3b) mixed anion perovskite solar cells show signs of degradation (lower  $V_{OC}$ ,  $J_{SC}$ , and FF). This information serves as a basic ground operation test, mimicking handling and transportation conditions that are common for large solar arrays before they are sent into space operation [43], [45]. Perovskite solar cell storage degradation is a common problem that has been noted in literature and can be remedied by improved packaging as well as compositional engineering [49], [66]. Nowadays encapsulation and packaging of the perovskite photovoltaics and their general stability is emerging as the next focal point of investigation in the perovskite research community [74], [75].

Next, space environment testing was performed under high vacuum and reduced temperature. JV measurements were done while the cell was being cooled down to  $-120\text{ }^{\circ}\text{C}$  under  $1 \times 10^{-7}$  Torr (Fig. 3c,d). General behavior of the solar cell could be split into three regions by temperature. No major changes to the device performance was observed in the range between  $25$  and  $-20\text{ }^{\circ}\text{C}$  (I). After  $-20\text{ }^{\circ}\text{C}$  and down to  $-90\text{ }^{\circ}\text{C}$ , FF of the solar cell decreases significantly (II), followed by an abrupt transition after  $-90\text{ }^{\circ}\text{C}$ . Here the JV curve flattens, showing very low  $J_{SC}$  value while still maintaining its  $V_{OC}$  (III). The temperature corresponding to the change in JV curve shape correlates closely with the temperature at which photoluminescence (PL) peak position of  $\text{CH}_3\text{NH}_3\text{PbI}_{3-x}\text{Cl}_x$  thin film starts to change [76]. The PL shift is explained by transition from tetragonal to orthorhombic crystal phase that occurs in this type of perovskite materials as a sample is cooled down [77]. This change of the crystal phase is associated with change in band gap, thus explaining difference in performance in this solar cell in low temperature regime. Upon closer examination of JV curves,  $V_{OC}$  (Fig. 3e) increases from  $890$  to  $940\text{ mV}$  between  $25$  and  $-20\text{ }^{\circ}\text{C}$ , decreases to  $930\text{ mV}$  at  $-90\text{ }^{\circ}\text{C}$  and then drops by about  $50\text{ mV}$  at temperatures below  $-90\text{ }^{\circ}\text{C}$  showing overall erratic behavior. Almost linear increase in the first temperature region is predicted by the following equation that is derived from the general diode model [78]:

$$qV_{OC} = E_A - nk_B T \ln \left( \frac{J_{00}}{J_{ph}} \right) \quad (2)$$

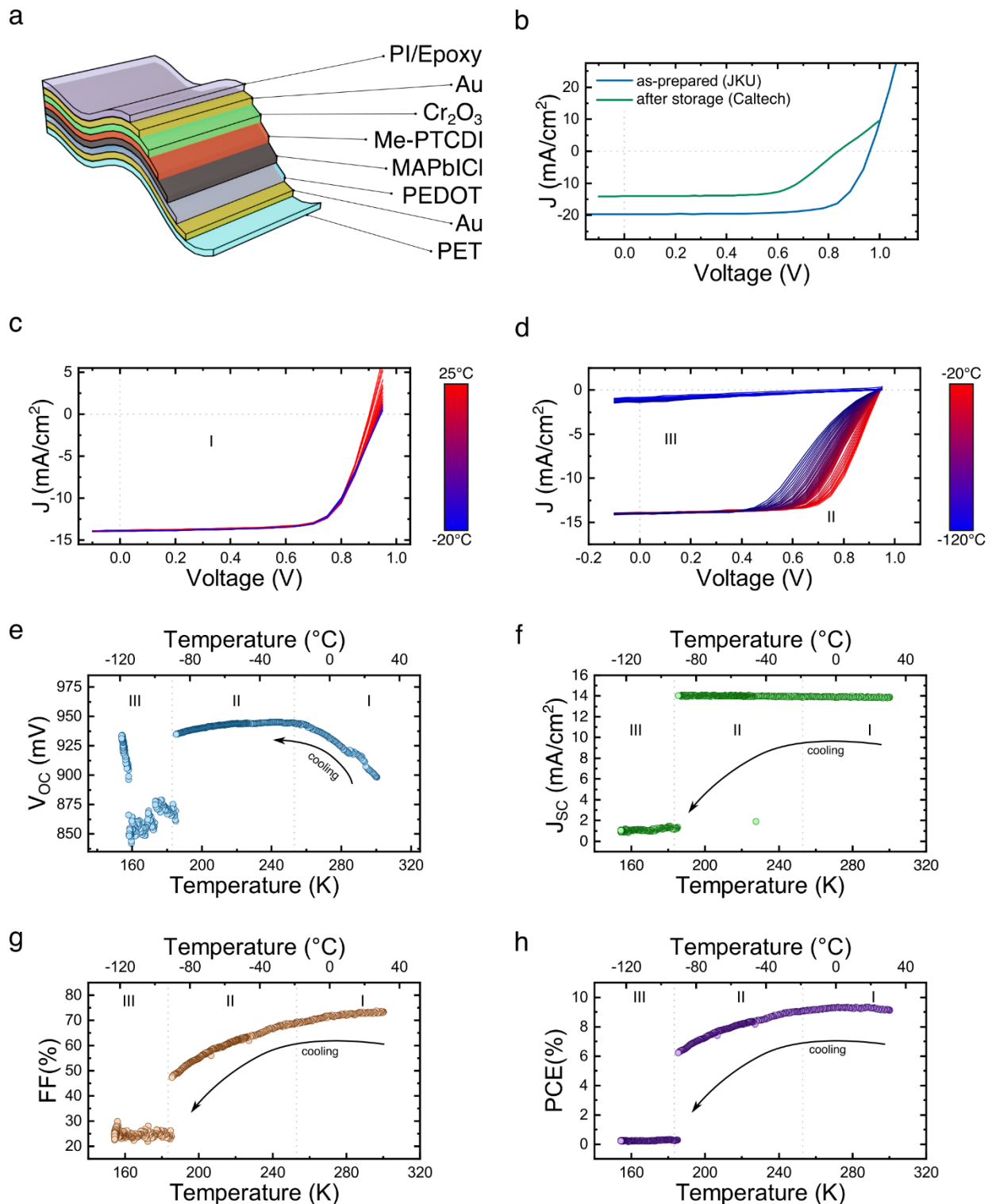


**Figure 3. JV characterization of mixed anion perovskite solar cells under low temperature conditions. (a)** Device architecture of ultra lightweight and flexible mixed anion perovskite solar cell fabricated on  $1.4\ \mu\text{m}$  PET foil, with  $\text{MAPbI}_{3-x}\text{Cl}_x$  in the middle, surrounded by hole and electron transporting layers (PEDOT and PTCDI respectively), chromium-gold electrode and encapsulated with PI and epoxy; **(b)** JV characteristics of a device measured right after

the fabrication and then later after transportation and storage, highlighting decrease in performance. JV measurements as a function of decreasing temperature in the range between **(c)** 25 and -20 °C and then between **(d)** -20 and -120 °C. Initially the cells do not show significant change in their JV behavior until -20 °C (I), then gradual FF decrease is observed between -20 and -90 °C (II), followed by noticeable drop of  $J_{sc}$  and FF after -90 °C due to crystal phase transition occurring in this type of perovskites (III). **(e)**  $V_{oc}$  as a function of decreasing temperature, shows initial increase (I) as predicted by theory, then relative saturation (II), and abrupt decrease (III) at lower temperatures. **(f)**  $J_{sc}$  as a function of decreasing temperature, demonstrating a steady value (I, II), up until -90 °C, where it decreases significantly. **(g)** FF as a function of decreasing temperature, monotonically decreasing with decreasing temperature (I, II) until -90 °C phase transition temperature, after which its value drastically drops. **(h)** Power conversion efficiency as a function of decreasing temperature, showing relatively stable value in the beginning (I), modest decrease after -20 °C (II), and instantaneous drop after -90 °C (III); (all measurements performed in high vacuum [ $10^{-7}$  Torr] and under AM1.5 illumination).

where  $q$  is the elementary charge,  $E_A$  – activation energy of the dominant recombination mechanism,  $n$  – ideality factor of the solar cell,  $k_B$  – Boltzmann constant,  $T$  – temperature,  $J_{00}$  – prefactor of the reverse saturation current density  $J_0$ , and  $J_{ph}$  – photocurrent density. By extrapolating the  $V_{oc}$  within the linear regime to 0 K it is possible to estimate  $E_A$ . In this case significant difference between the estimated  $E_A$  and the band gap of  $CH_3NH_3PbI_{3-x}Cl_x$  ( $E_A \approx 1.3$  eV and  $E_g \approx 1.5$  eV) suggests the non-radiative recombination path at interfaces of the perovskite active material [79], [80]. Nevertheless, it is important to mention that extrapolating from the limited set of data at higher temperatures introduces uncertainty that is at least  $\pm 0.1$  V.  $V_{oc}$  saturation at around 200 K was previously observed in different thin film photovoltaics studies including perovskites [80]–[82], OPV [83], and CZTSSe [84]. This saturation region suggests that there are different factors limiting  $V_{oc}$  in various temperature regions:  $T > 200$  K - interfacial charge recombination,  $T < 200$  K - low charge carrier transfer rate [81], [83].  $J_{sc}$  appears to remain relatively stable up until phase transition temperature where it drops by an order of magnitude (Fig. 3f), whereas FF slowly decreases from 70 to 50 % up until -90 °C (Fig. 3g). Overall, power conversion efficiency remains stable between 25 and -20 °C, with best performance at around 0 °C, and drops by about 30 % between -20 and -90 °C (Fig. 3h). Crystal phase transition effectively limits device performance at temperatures below -90 °C. It has been previously reported that problems with charge carrier extraction in the electron transporting layer is the main reason for subpar performance of these type of perovskite solar cells at low temperatures [49], [85]. Nonetheless, it appears that the issue can be resolved by either doping the existing electron

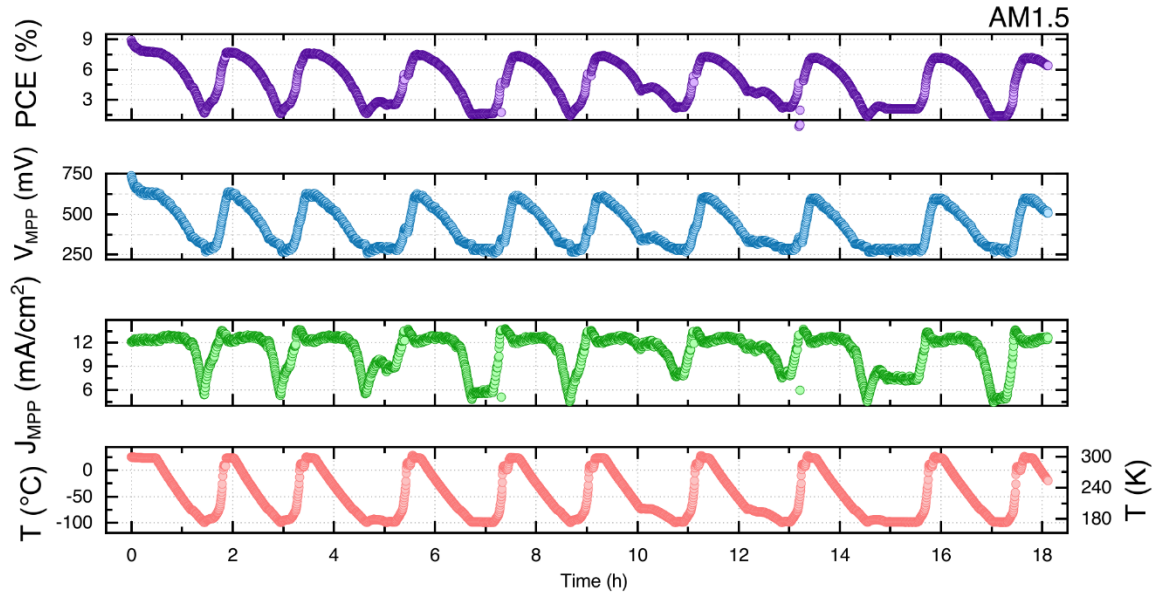


**Figure 4. Maximum power point tracking of mixed anion perovskite solar cells.** Power conversion efficiency (purple) and corresponding  $V_{MPP}$  (blue) and  $J_{MPP}$  (green) values as a function of varying temperature conditions (pink) over the period of 18 h (9 cycles) under constant illumination (AM1.5) and high vacuum ( $10^{-7}$  Torr).

transporting layer or replacing it with more conductive alternatives which allow the solar cell to perform well under low temperature conditions.

Even though performance of mixed anion solar cell is poor at low temperature, this behavior is reversible when the temperature is brought back up. In order to confirm this hypothesis, vacuum thermal cycling between 25 and -100 °C at  $1 \times 10^{-7}$  Torr and under constant AM1.5 illumination with maximum power point tracking was performed. As it is evident in Fig. 4, power conversion efficiency starts at 9 %, has a small initial “burn-in” period and continues to drop as the temperature decreases. Nevertheless, it recovers when the temperature is brought back to 25 °C and keeps on recovering for another 8 temperature cycles.

In order to access the effects of high temperatures on flexible mixed anion perovskite solar cells, JV sweeps were measured as the temperature was increased stepwise up to 80 °C.  $V_{OC}$  is most sensitive to changes in temperature (Fig. 5a). As expected from eq. 2,  $V_{OC}$  decreases with increasing temperature but tends to return to its original value when the temperature is decreased again.  $V_{OC}$  value does not recover sufficiently after 60 °C.  $J_{SC}$  remains stable up until 70 °C but does recover relatively quickly even when the cell is heated to 80 °C (Fig. 5b). FF remains unperturbed up until 60 °C and appears to deteriorate after

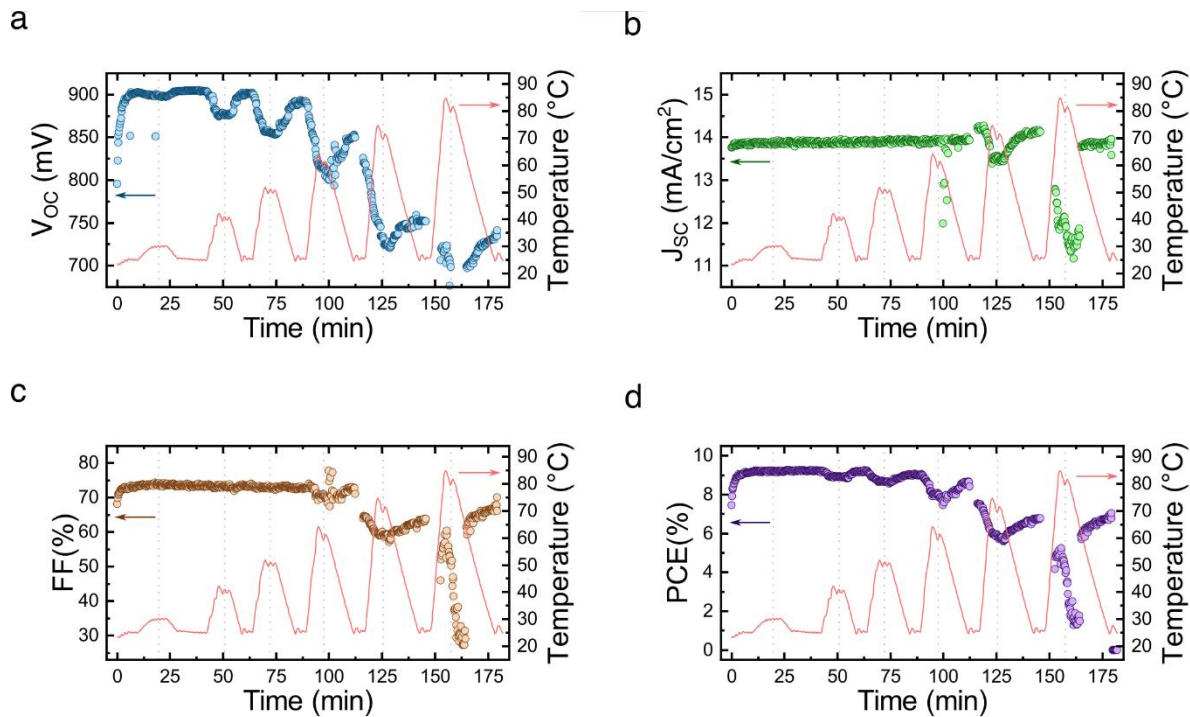


**Figure 5. Solar cell parameters of mixed anion perovskite solar cell during dynamic stepwise temperature increase. (a)**  $V_{oc}$  showing high sensitivity to temperature changes, starts to slightly decrease already at 40 °C and exhibits signs of recovery up to 60 °C. Significant decrease and later poor recovery is observed after 70 °C. **(b)**  $J_{sc}$  shows stable behavior up to 60 °C, then decreases with swift recovery up to 80 °C; **(c)** FF displays robust values up until 60 °C and reasonable recovery up to 80 °C. **(d)** Power conversion efficiency does not decrease significantly up until 50 °C. While heated to 60-70 °C and higher the solar cells exhibits some degree of recovery but overall lower performance; (all measurements performed in high vacuum [ $10^{-6}$ - $10^{-7}$  torr] and under AM1.5 illumination).

the sample is heated to 80 °C (Fig. 5c). Overall the cell efficiency starts to show worse performance after heating to above 60-70 °C and does not recover in a short period of time (Fig. 5d). Effects of thermal cycling on rigid perovskite solar cell stability have been previously reported, highlighting the importance of charge transport layer selection and showing recovery after a number of cycles (anywhere from 10 to 200) even if heated to 80 °C [86]–[89].

Curiously, during post-test investigation it was observed that PET supporting frame has undergone some permanent mechanical deformation (bending out of plane), most likely due to changes in mechanical properties of this material around its glass transition point. This is very likely the cause of bad electrical contact and therefore missing data points at around 112, 150, and 162 min. These results suggest that

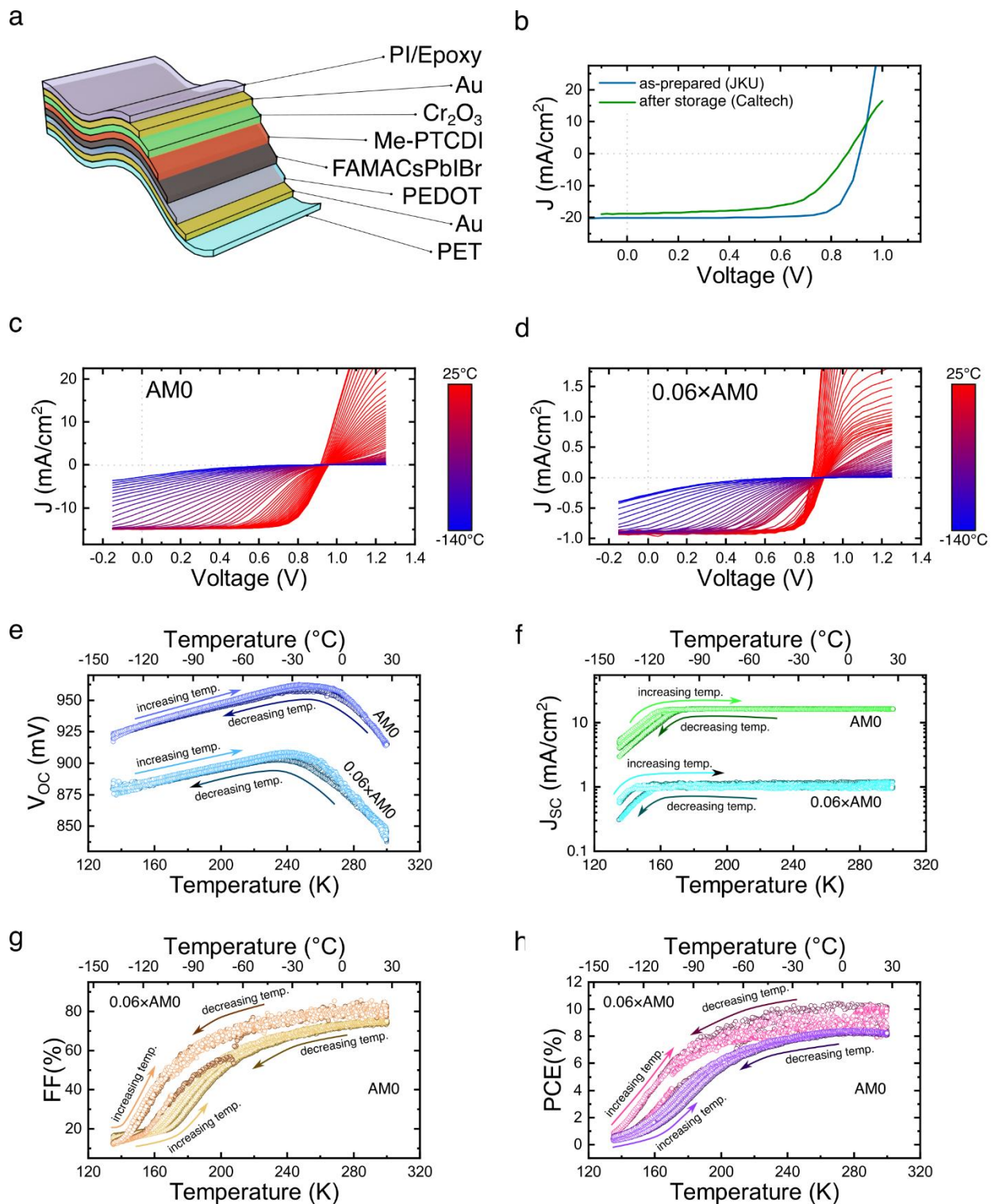


**Figure 6. JV characterization of mixed cation - mixed anion perovskite solar cells under low temperature - low intensity cycling conditions. (a)** Device architecture of the solar cell with  $\text{Cs}_{0.05}(\text{FA}_{0.83}\text{MA}_{0.17})_{0.95}\text{PbI}_{3-x}\text{Br}_x$  as its active material; **(b)** JV sweeps of the solar cell right after fabrication at JKU and after before low temperature measurement at Caltech, highlighting deterioration of its performance due to storage and transport. Both JV measurements were

done under AM1.5 illumination. JV sweeps measured at **(c)** AM0 and **(d)** 0.06×AM0 (approximate fraction of solar light reaching Jupiter) illumination as a function of decreasing temperature between 25 and -140 °. No crystal phase transition is observed underlining this perovskite composition as the leading material for space application; **(e)**  $V_{oc}$  **(f)**  $J_{sc}$  **(g)** FF **(h)** power conversion efficiency for samples illuminated at AM0 and 0.06×AM0 as the temperature was cycled in the range between 25 and -140 °C four times.

mechanical support for the prototype cells needs to be replaced with more thermally stable material. Nevertheless, relatively low loss of power conversion efficiency (about 75 % of its initial value after several heating cycles) is a sign of both promising thermal and mechanical performance.

### Mixed cation mixed anion solar cells low intensity – low light testing

The next set of vacuum thermal cycling experiments were performed on mixed cation - mixed anion perovskites flexible solar cells (Fig. 6a). Similar to mixed anion perovskite solar cells, these devices exhibit some degradation after transport and storage, though to a lesser extent, confirming generally higher performance of this perovskite composition (Fig. 6b). One set of thermal cycling was performed under high intensity illumination AM0, while another was done under low intensity illumination 0.06×AM0. JV sweeps recorder under AM0 illumination show initially good performance that decreases after lowering the temperature down to -140 °C (Fig. 6c). As opposed to mixed anion perovskite solar cells, this composition does not show any crystal phase transition features in the measured temperature region, therefore confirming that it is better suited for low temperature operation [48], [49], [67], [90]. This makes mixed cation - mixed anion perovskite solar a better candidate for space applications. When measured under 0.06×AM0 and low temperature, conditions resembling those of Jupiters orbit, the cells show initially better performance that also decreases when the temperature is brought down to -140 °C (Fig. 6d). Improved performance under low illumination intensity can be ascribed to improved balance between photogeneration and extraction of charge carriers [85]. Eventual decrease in performance of these cells under low intensity – low temperature as well as lower current in forward bias regime might be due to parasitic energetic barrier at the interface of perovskite active material and electron transporting layer. This might be caused by band misalignment or low conductivity of the electron transporting layer [49], [85]. As in mixed anion perovskite solar cells,  $V_{oc}$  of these samples has a region of initial linear increase when the temperature is decreased, followed by saturation and then slow decrease (Fig. 6e). It is important to note, that even after the saturation and decrease of  $V_{oc}$ , the value at low

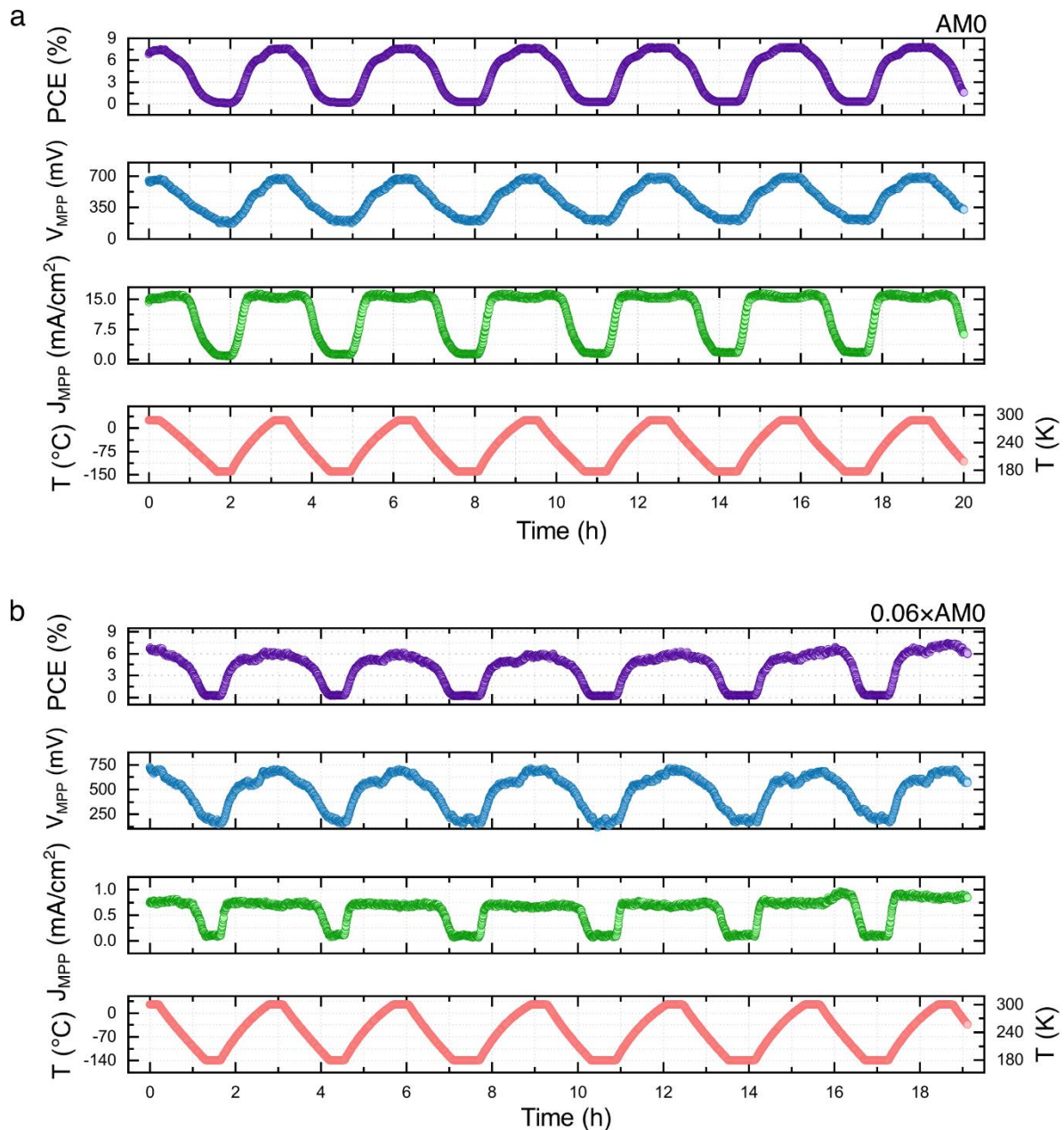


**Figure 7. Maximum power tracking analysis of mixed cation - mixed anion perovskite solar cells.** Maximum power point tracking was performed under **(a)** high intensity (AM0) and **(b)** low intensity light (0.06×AM0) while monitoring power conversion efficiency,  $V_{MPP}$ , and  $J_{MPP}$ . The temperature was cycled in range between 25 and -140 °C for 20 h (6.5 cycles).

temperatures is still about the same (AM0, ~920 mV) or even higher (0.06×AM0, ~875 mV) than initial value at 25 °C (AM0 ~ 920 mV, 0.06×AM0 ~825 mV). Additionally,  $V_{OC}$  saturation point occurs at lower

temperatures for the cell measured at 0.06×AM0 (*ca.* 220 K) when compared to cells measured at AM0 (*ca.* 240 K), once again implying better performance of mixed cation - mixed anion perovskites in low intensity – low temperature conditions. Using eq. 2,  $E_a$  values were extrapolated, showing difference  $\sim 0.2$  eV difference between  $E_g$  ( $\sim 1.6$  eV) and  $E_a$  ( $\sim 1.4$  eV). Difference in  $V_{oc}$  at lower versus higher illumination intensities is in line with theoretical predictions and previous reports, where it has been shown that  $V_{oc}$  decreases with decreasing light intensity in logarithmic manner [80].  $J_{sc}$  remains stable down to very low temperatures (Fig. 6f). The temperature at which  $J_{sc}$  starts to decrease rapidly, varies between high intensity and low intensity light, with samples operating under 0.06×AM0 having stable  $J_{sc}$  down to *ca.*  $-130$  °C, and AM0 samples showing rapid decrease in  $J_{sc}$  already at *ca.*  $-110$  °C. This can be explained by smaller number of photogenerated carriers at lower light intensity resulting in better extraction of charge carriers and smaller series resistance. As mentioned before, FF slowly deteriorates as the temperature decreases, likely due to poor charge transport in PEDOT (p-type) and/or PTCDI (n-type) layers cause by carrier freeze out (Fig. 6g). Higher FF values at lower light intensities can also be attributed to improved balance between charge carrier generation and extraction. Power conversion efficiency remains relatively stable down to  $-30$  °C for AM0 illuminated samples and down to  $-50$  °C for 0.06×AM0 samples. Additionally, power conversion efficiency is higher in low light intensity conditions when compared to AM0 conditions. Nevertheless, in both situations it is still showing poor performance at very low temperatures (Fig. 6h).

In order to test mixed cation - mixed anion perovskites solar cell within longer time frame, vacuum thermal cycling at maximum power point experiment was performed. The temperature was varied between 25 and  $-140$  °C for both high (Fig. 7a) and low intensity (Fig. 7b) light illumination conditions. Both experiments ran for 6 thermal cycles and show that the cells recover well after thermal cycling with samples under low intensity light showing a bit larger window of high power conversion efficiency.

#### Mixed cation mixed anion solar cell low Earth orbit simulation

In order to ascertain the performance of mixed cation - mixed anion perovskites solar cells under more complex conditions, where both temperature and light conditions change over time, a simplified orbital operation simulation was performed. Every space mission is defined by its trajectory and for Earth orbiting they are approximately grouped into low Earth orbit (LEO, 300-900 km), mid-Earth orbit (MEO, *ca.* 20000 km), geosynchronous (GEO, *ca.* 35000 km), and highly elliptical orbit (HEO, 200-1500 km). For this simulation low Earth orbit trajectory was chosen due to its relatively short orbital period (*ca.* 130 min) and the fact that majority of satellites are currently residing in it. The orbit simulation in this study involves

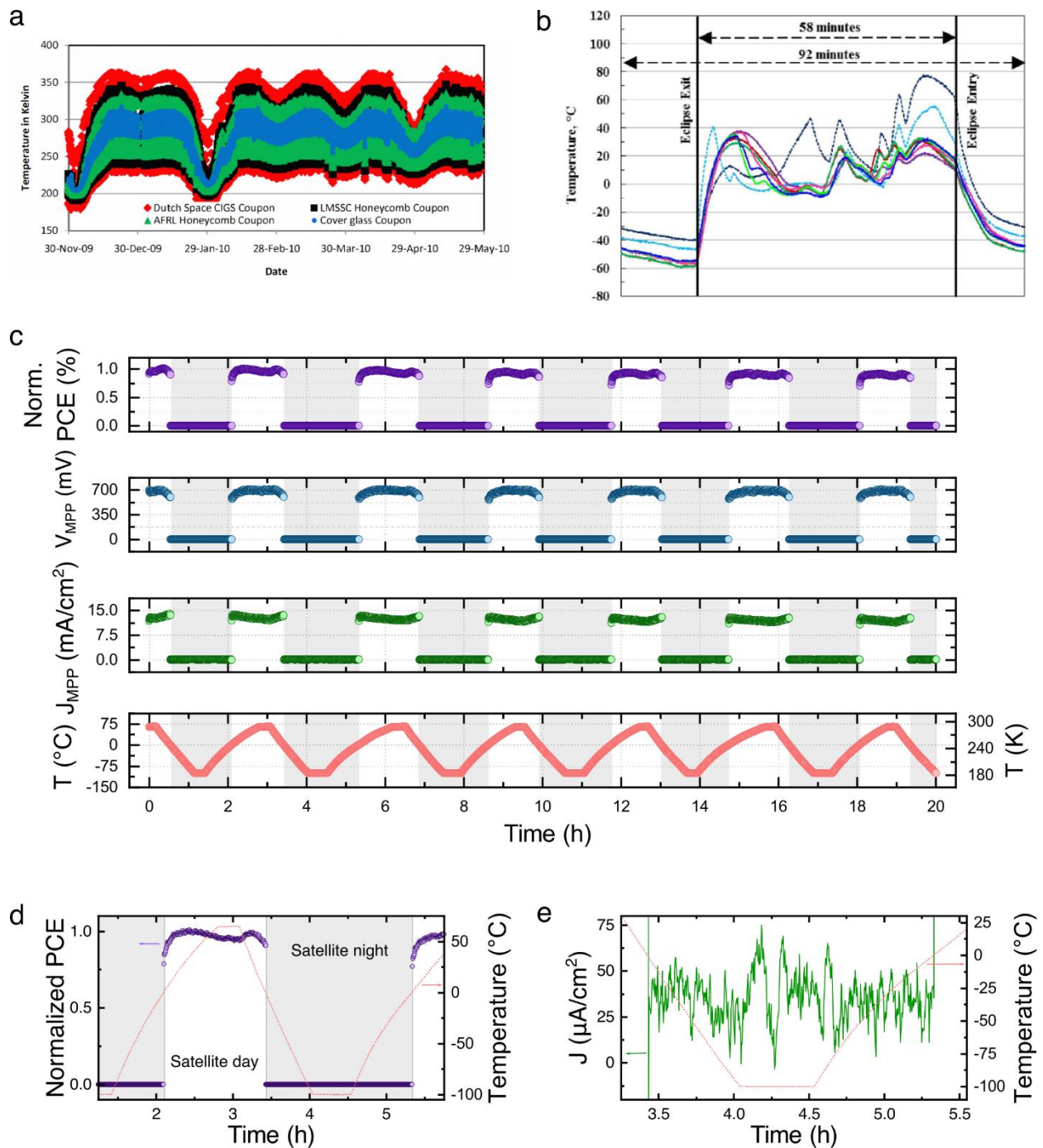


**Figure 8. Low Earth orbit simulation experiment. (a)** Temperature variations experienced by different solar cell coupons during the second Forward Technology Solar Cell Experiment (FTSCE) [between November 30, 2009 and May 29, 2010] on board of International Space Station [91]. Differently colored lines refer to different solar power modules located on the array. **(b)** Temperature profile of Roll-Out Solar Array (ROSA) during on-orbit validation [52]. **(c)** Maximum power point tracking performance of mixed cation - mixed anion perovskite solar cell under simulated low Earth orbit conditions. Gray areas signify the period during which the solar simulator (AM0) was turned off (“satellite night”) and kept under short circuit conditions. **(d)** Four hours highlight of low Earth orbit simulation,

showing power conversion efficiency as a function of temperature and illumination. **(e)** Maximum power point current density during an example “satellite night” of the low Earth orbit simulation cycle showing no significant difference in temperature range between 0 and -100 °C.

temperature cycling with periodic light illumination. Using data available from previous missions that focused on performance of photovoltaic technology in space, it was possible to estimate conditions a solar cell might experience in low Earth orbit. The second Forward Technology Solar Cell Experiment (FTSCE) focused on testing a number of different thin film photovoltaic technologies (multijunction solar cells, amorphous Si, CIGS) on board of International Space Station as a part of Materials on the International Space Station Experiment 7 (MISSE7) [91]. Thermal environment data was reported, showing that the devices can experience temperatures in range between -100 and 80 °C depending on solar exposure and thermal contact with the cell (Fig. 8a). Based on results available Roll-Out Space Array (ROSA) testing on International Space Station, typical exposure to Sun would be around 60 min and the eclipse (dark period) would last for about 30 min (Fig. 8b). Considering information from past missions, previous thermal tests of perovskite solar cells in this study, and limitations of the experimental set-up, a simulated low Earth orbit test profile was designed. Maximum temperature was set to 65 °C, minimum temperature was set to -100 °C, “satellite day” lasted for about 90 min (0 - 65 - 0 °C), and “satellite night” for about 90 min (0 - -100°C - -0 °C). During the “satellite day” the cell was kept under maximum power point tracking conditions and during “satellite night” it was kept under short circuit conditions. Power conversion efficiency of the cell after 6.5 low Earth orbit day-night cycles maintains 90 % of its original value (Fig. 8c). In general, this is a promising result, that will require further investigation to clarify if additional day - night cycles will cause further degradation of cells performance or if these devices will settle at a steady, but lower-than-initial, value. Upon closer examination, it appears that the cell has its best performance at around 35 to 40 °C and has about 95 % of its initial value at 65 °C. Prompt recovery was observed when the temperature of the cell started to decrease again (Fig. 8d). As mentioned before, during the “satellite night” phase of the simulation the cell was kept under short circuit conditions. It appears that dark short circuit current does not change significantly regardless of temperature variation (Fig. 8e). During post-test examination small amounts of supporting frame deformation was observed, similar to high temperature test done on mixed anion perovskite solar cells. In this case, it did not cause any electrical contact issues, but further supports the case of mechanical resilience of ultra lightweight perovskite solar cells.

## Conclusions and Outlook

This three-months research visit resulted in first-of-its-kind space environment examination of performance and stability of flexible ultra lightweight perovskite solar cells. Devices were fabricated using two compositions of perovskite absorber (mixed anion and mixed cation – mixed anion perovskite) and were tested at high vacuum and range of temperatures between -140 and 80 °C. Mixed anion devices, in addition to more pronounced degradation during transport and storage, showed abrupt decrease in performance due to crystal phase transition of this active material composition at low temperatures. Nevertheless, the change appears to be reversible and the cells operated successfully after 9 thermal cycles over the period of 18 h. Additionally, a short examination of high temperature performance of mixed anion perovskite solar cells was done, suggesting that 65-70 °C might be the maximum temperature at which these cells can operate with no severe damage. The study of the better performing mixed cation – mixed anion perovskite ultra lightweight solar cells that mimicked low intensity – low temperature conditions showed good performance with no abrupt changes at low temperature. Nonetheless, at temperatures below -70 °C these devices show worse performance, most likely due to charge carrier freeze out. All the changes to the cells' operation were also reversible when the temperature was raised again and they maintained their performance for 18 h over 6 thermal cycles. Interestingly, mixed cation – mixed anion perovskite solar cells also showed better performance at low intensity conditions. Further testing under simulated low Earth orbit conditions showed good performance for about 18 to 20 h with only very little decrease in efficiency. Overall this is a promising outcome, demonstrating potential use of ultra lightweight perovskites in the field of aerospace.

Moving forward, we plan to not only perform further tests on these solar cells but also work on improving their architecture in order to address some of the performance issues at low temperatures. One of the first tests to come will be radiation testing, that was planned for this visit but was unfortunately postponed due scheduling issues. Other tests will include increased number of day-night cycles in simulated low Earth orbit conditions, and external quantum efficiency (EQE) measurements under low intensity – low light conditions at dedicated equipment of Jet Propulsion Laboratory managed California Institute of Technology. In order to address reduced performance under low intensity – low light conditions we plan to focus our further research on charge carrier and interface engineering, choosing electron and hole transporting layers that are better suited for this range of temperatures. Additionally, we plan to optimize perovskite formulations in order to reduce degradation during transportation and storage. From an engineering standpoint, the underlying mechanical and electrical challenges will also need to be resolved to intimately integrate these devices into arrays and deployable structures.

This study together with other examples in literature provides a strong case for perovskite solar cells in ultra lightweight format in aerospace application. Furthermore, successful outcomes from these efforts will benefit not only aerospace technology, but also a number of other fields such as robotics, environmental monitoring, agriculture, search and rescue missions, wearables for medical, sport and leisure applications. These opportunities for improvement and broad merit to numerous branches of science provide powerful motivation to further investigate the field of ultra lightweight perovskite solar cells and continue this collaboration between JKU and Caltech.

## Bibliography

- [1] A. K. Jena, A. Kulkarni, and T. Miyasaka, "Halide Perovskite Photovoltaics: Background, Status, and Future Prospects," *Chem. Rev.*, vol. 119, no. 5, pp. 3036–3103, 2019, doi: 10.1021/acs.chemrev.8b00539.
- [2] A. R. Chakhmouradian and P. M. Woodward, "Celebrating 175 years of perovskite research: A tribute to Roger H. Mitchell," *Phys. Chem. Miner.*, vol. 41, no. 6, pp. 387–391, 2014, doi: 10.1007/s00269-014-0678-9.
- [3] M. Johnsson and P. Lemmens, "Crystallography and chemistry of perovskites," *Arxiv.org*, 2005.
- [4] C. N. R. Rao, "Perovskite oxides and high-temperature superconductivity," *Ferroelectrics*, vol. 102, no. 1, pp. 297–308, 1990, doi: 10.1080/00150199008221489.
- [5] N. Yanase, K. Abe, N. Fukushima, and T. Kawakubo, "Thickness dependence of ferroelectricity in heteroepitaxial BaTiO<sub>3</sub> thin film capacitors," *Japanese J. Appl. Physics, Part 1 Regul. Pap. Short Notes Rev. Pap.*, vol. 38, no. 9 B, pp. 5305–5308, 1999, doi: 10.1143/jjap.38.5305.
- [6] K. Uchino, "Glory of piezoelectric perovskites," *Sci. Technol. Adv. Mater.*, vol. 16, no. 4, 2015, doi: 10.1088/1468-6996/16/4/046001.
- [7] J. A. Mareš, N. Čechová, M. Nikl, J. Kvapil, R. Krátký, and J. Pospíšil, "Cerium-doped RE<sub>3</sub>+AlO<sub>3</sub> perovskite scintillators: Spectroscopy and radiation induced defects," *J. Alloys Compd.*, vol. 275–277, pp. 200–204, 1998, doi: 10.1016/S0925-8388(98)00303-X.
- [8] J. Hwang, R. R. Rao, L. Giordano, Y. Katayama, Y. Yu, and Y. Shao-Horn, "Perovskites in catalysis and electrocatalysis," *Science (80-. )*, vol. 358, no. 6364, pp. 751–756, 2017, doi: 10.1126/science.aam7092.
- [9] B. Raveau, A. Maignan, C. Martin, and M. Hervieu, "Colossal Magnetoresistance Manganite Perovskites: Relations between Crystal Chemistry and Properties," *Chem. Mater.*, vol. 10, no. 10, pp. 2641–2652, 1998, doi: 10.1021/cm9801791.
- [10] H. Y. Ye *et al.*, "Metal-free three-dimensional perovskite ferroelectrics," *Science (80-. )*, vol. 361, no. 6398, pp. 151–155, 2018, doi: 10.1126/science.aas9330.
- [11] H. Liu and X. Yang, "A brief review on perovskite multiferroics," *Ferroelectrics*, vol. 507, no. 1, pp. 69–85, 2017, doi: 10.1080/00150193.2017.1283171.
- [12] H. Wells, "Über die Cäsium-und Kalium-Bleihalogenide," *Zeitschrift für Anorg. Chemie*, pp. 195–210, 1893.
- [13] C.K. Moller, "Crystal Structure and Photoconductivity of Caesium Plumbohalides," *Nature*, vol. 182, no. 1955, p. 1436, 1958.
- [14] D. Weber, "CH<sub>3</sub>NH<sub>3</sub>PbX<sub>3</sub>, ein Pb(II)-System mit kubischer Perowskitstruktur / CH<sub>3</sub>NH<sub>3</sub>PbX<sub>3</sub>, a Pb(II)-System with Cubic Perovskite Structure," *Zeitschrift für Naturforsch. B*, 1978.
- [15] A. Kojima, K. Teshima, Y. Shirai, and T. Miyasaka, "Organometal halide perovskites as visible-light sensitizers for photovoltaic cells," *J. Am. Chem. Soc.*, vol. 131, no. 17, pp. 6050–6051, 2009, doi: 10.1021/ja809598r.
- [16] M. Lee, J. Teuscher, T. Miyasaka, T. Murakami, and H. Snaith, "Efficient hybrid solar cells based on meso-structured organometal halide perovites," *Science (80-. )*, vol. 338, no. November, pp. 643–648, 2012.
- [17] M. Kaltenbrunner *et al.*, "Flexible high power-per-weight perovskite solar cells with chromium oxide-metal contacts for improved stability in air," *Nat. Mater.*, vol. 14, no. 10, pp. 1032–1039, 2015, doi: 10.1038/nmat4388.
- [18] M. Gaskill, "Changing How Solar Power Rolls," *International Space Station Program Office, NASA Johnson Space Center*, 2017. [Online]. Available: [https://www.nasa.gov/mission\\_pages/station/research/news/changing-how-solar-power-rolls](https://www.nasa.gov/mission_pages/station/research/news/changing-how-solar-power-rolls). [Accessed:

01-Jan-2020].

- [19] Jeremy A. Banik, "Roll-Out Space Array," *NASA Investigations, Facilities and Publications*. [Online]. Available: [https://www.nasa.gov/mission\\_pages/station/research/experiments/explorer/Investigation.html?id=1876](https://www.nasa.gov/mission_pages/station/research/experiments/explorer/Investigation.html?id=1876). [Accessed: 02-Jan-2020].
- [20] P. Beauchamp, R. Ewell, E. Brandon, and R. Surampudi, "Solar Power and Energy Storage for Planetary Missions," *Jet Propulsion Laboratory and California Institute of Technology*, vol. 2015, no. c. NASA, 2015.
- [21] V. Goldschmidt, "Die gesetze der krystallochemie. Naturwissenschaften," *Naturwissenschaften*, pp. 477–85, 1926.
- [22] Q. Van Le, H. W. Jang, and S. Y. Kim, "Recent Advances toward High-Efficiency Halide Perovskite Light-Emitting Diodes: Review and Perspective," *Small Methods*, vol. 2, no. 10, p. 1700419, 2018, doi: 10.1002/smt.201700419.
- [23] H. Wei and J. Huang, "Halide lead perovskites for ionizing radiation detection," *Nat. Commun.*, vol. 10, no. 1, pp. 1–12, 2019, doi: 10.1038/s41467-019-08981-w.
- [24] X. Zhao, H. Xu, Z. Wang, Y. Lin, and Y. Liu, "Memristors with organic-inorganic halide perovskites," *InfoMat*, no. April, pp. 183–210, 2019, doi: 10.1002/inf2.12012.
- [25] P. Brody and D. Page, "Flexible thin-film transistors stretch performance, shrink cost(Thin film transistors fabrication from flexible substrates, discussing heat conductivity, properties and costs)," *Electronics*, 1968.
- [26] K. A. Ray, "Flexible solar cell arrays for increased space power," *IEEE Trans. Aerosp. Electron. Syst.*, vol. 3, no. 1, 1967.
- [27] S. D. Theiss and S. Wagner, "Amorphous silicon thin-film transistors on steel foil substrates," *IEEE Electron Device Lett.*, vol. 17, no. 12, pp. 578–580, 1999, doi: 10.1109/55.545776.
- [28] T. Someya, S. Bauer, and M. Kaltenbrunner, "Imperceptible organic electronics," *MRS Bull.*, vol. 42, no. 2, pp. 124–130, 2017, doi: 10.1557/mrs.2017.1.
- [29] M. Kaltenbrunner *et al.*, "An ultra-lightweight design for imperceptible plastic electronics," *Nature*, vol. 499, no. February 2013, pp. 458–463, 2013, doi: 10.1038/nature12314.
- [30] M. S. White *et al.*, "Ultrathin, highly flexible and stretchable PLEDs," *Nat. Photonics*, vol. 7, no. 10, pp. 811–816, 2013, doi: 10.1038/nphoton.2013.188.
- [31] M. Kaltenbrunner *et al.*, "Ultrathin and lightweight organic solar cells with high flexibility," *Nat. Commun.*, 2012, doi: 10.1038/ncomms1772.
- [32] B. J. Kim *et al.*, "Highly efficient and bending durable perovskite solar cells: Toward a wearable power source," *Energy Environ. Sci.*, vol. 8, no. 3, pp. 916–921, 2015, doi: 10.1039/c4ee02441a.
- [33] Z. Wen *et al.*, "Self-powered textile for Wearable electronics by hybridizing fiber-shaped nanogenerators, solar cells, and supercapacitors," *Sci. Adv.*, vol. 2, no. 10, 2016, doi: 10.1126/sciadv.1600097.
- [34] C. García Núñez, L. Manjakkal, and R. Dahiya, "Energy autonomous electronic skin," *npj Flex. Electron.*, vol. 3, no. 1, 2019, doi: 10.1038/s41528-018-0045-x.
- [35] D. Yang, R. Yang, S. Priya, and S. (Frank) Liu, "Recent Advances in Flexible Perovskite Solar Cells: Fabrication and Applications," *Angew. Chemie - Int. Ed.*, vol. 58, no. 14, pp. 4466–4483, 2019, doi: 10.1002/anie.201809781.
- [36] C. Y. Chen, J. H. Chang, K. M. Chiang, H. L. Lin, S. Y. Hsiao, and H. W. Lin, "Perovskite Photovoltaics for Dim-Light Applications," *Adv. Funct. Mater.*, vol. 25, no. 45, pp. 7064–7070, 2015, doi:

- 10.1002/adfm.201503448.
- [37] R. Søndergaard, M. Hösel, D. Angmo, T. T. Larsen-Olsen, and F. C. Krebs, "Roll-to-roll fabrication of polymer solar cells," *Mater. Today*, vol. 15, no. 1–2, pp. 36–49, 2012, doi: 10.1016/S1369-7021(12)70019-6.
- [38] J. C. Tinguely, R. Solarska, A. Braun, and T. Graule, "Low-temperature roll-to-roll coating procedure of dye-sensitized solar cell photoelectrodes on flexible polymer-based substrates," *Semicond. Sci. Technol.*, vol. 26, no. 4, 2011, doi: 10.1088/0268-1242/26/4/045007.
- [39] C. Zhang *et al.*, "Efficient and Flexible Thin Film Amorphous Silicon Solar Cells on Nanotextured Polymer Substrate Using Sol-gel Based Nanoimprinting Method," *Adv. Funct. Mater.*, vol. 27, no. 13, 2017, doi: 10.1002/adfm.201604720.
- [40] D. Scheiman *et al.*, "High efficiency flexible triple junction solar panels," *2014 IEEE 40th Photovolt. Spec. Conf. PVSC 2014*, vol. 2, pp. 1376–1380, 2014, doi: 10.1109/PVSC.2014.6925174.
- [41] A. Salavei *et al.*, "Comparison of high efficiency flexible CdTe solar cells on different substrates at low temperature deposition," in *Solar Energy*, vol. 139, no. September, 2016, pp. 13–18.
- [42] E. Gilioli *et al.*, "CIGS-based flexible solar cells," in *Factories of the Future: The Italian Flagship Initiative*, Springer International Publishing, 2019, pp. 365–382.
- [43] S. Bailey and R. Raffaele, "Operation of Solar Cells in a Space Environment," in *Practical Handbook of Photovoltaics*, Elsevier Ltd, 2012, pp. 863–880.
- [44] R. Easton and M. Votaw, "Vanguard IIGY Satellite (1958 Beta)," *Rev. Sci. Instrum.*, vol. 30, no. 2, pp. 70–75, 1959.
- [45] E. F. Lisbona, "Calibration, Testing, and Monitoring of Space Solar Cells," in *Practical Handbook of Photovoltaics*, Elsevier Ltd, 2012, pp. 881–913.
- [46] S. F. Dawson, P. Stella, W. McAlpine, and B. Smith, "JUNO photovoltaic power at jupiter," *10th Annu. Int. Energy Convers. Eng. Conf. IECEC 2012*, no. August 2012, 2012, doi: 10.2514/6.2012-3833.
- [47] M. F. Piszczor *et al.*, "Advanced solar cell and array technology for NASA deep space missions," *Conf. Rec. IEEE Photovolt. Spec. Conf.*, 2008, doi: 10.1109/PVSC.2008.4922856.
- [48] J. Barbe *et al.*, "In situ investigation of perovskite solar cells' efficiency and stability in a mimic stratospheric environment for high altitude pseudo satellites," *J. Mater. Chem. C*, 2020, doi: 10.1039/c9tc04984c.
- [49] C. R. Brown, G. E. Eperon, V. R. Whiteside, and I. R. Sellers, "Potential of high-stability perovskite solar cells for low-intensity-low-temperature (LILT) outer planetary space missions," *ACS Appl. Energy Mater.*, vol. 2, no. 1, pp. 814–821, 2019, doi: 10.1021/acsaem.8b01882.
- [50] M. D. Kelzenberg *et al.*, "Design and Prototyping Efforts for the Space Solar Power Initiative," in *2018 6th IEEE International Conference on Wireless for Space and Extreme Environments (WiSEE)*, 2018, pp. 558–561, doi: 10.1109/PVSC.2017.8366621.
- [51] M. Garcia and B. Dunbar, "About the Space Station Solar Arrays," *National Aeronautics and Space Administration*, 2020. [Online]. Available: [https://www.nasa.gov/mission\\_pages/station/structure/elements/solar\\_arrays-about.html](https://www.nasa.gov/mission_pages/station/structure/elements/solar_arrays-about.html).
- [52] J. Banik, S. Kiefer, M. Lapointe, and P. Lacorte, "On-orbit validation of the roll-out solar array," *IEEE Aerosp. Conf. Proc.*, vol. 2018-March, pp. 1–9, 2018, doi: 10.1109/AERO.2018.8396390.
- [53] E. E. Gdoutos, C. Leclerc, F. Royer, D. Türk, and S. Pellegrino, "Ultralight Spacecraft Structure Prototype," in *AIAA Scitech 2019 Forum*, 2019, no. January, doi: 10.2514/6.2019-1749.
- [54] L. Hall and B. Dunbar, "STMD: Small Spacecraft Technology," *National Aeronautics and Space*

- Administration*, 2019. [Online]. Available: [https://www.nasa.gov/directorates/spacetech/small\\_spacecraft/smallsat\\_overview.html](https://www.nasa.gov/directorates/spacetech/small_spacecraft/smallsat_overview.html).
- [55] D. Williams, "Planetary Fact Sheet - Metric," *NASA Goddard Space Flight Center*, 2015. [Online]. Available: <http://nssdc.gsfc.nasa.gov/planetary/factsheet/>.
- [56] Y. Miyazawa, M. Ikegami, T. Miyasaka, T. Ohshima, M. Imaizumi, and K. Hirose, "Evaluation of radiation tolerance of perovskite solar cell for use in space," *2015 IEEE 42nd Photovolt. Spec. Conf. PVSC 2015*, pp. 1–4, 2015, doi: 10.1109/PVSC.2015.7355859.
- [57] Y. Miyazawa *et al.*, "Tolerance of Perovskite Solar Cell to High-Energy Particle Irradiations in Space Environment," *iScience*, vol. 2, pp. 148–155, 2018, doi: 10.1016/j.isci.2018.03.020.
- [58] F. Lang *et al.*, "Radiation Hardness and Self-Healing of Perovskite Solar Cells," *Adv. Mater.*, vol. 28, no. 39, pp. 8726–8731, 2016, doi: 10.1002/adma.201603326.
- [59] F. Lang *et al.*, "Efficient minority carrier detrapping mediating the radiation hardness of triple-cation perovskite solar cells under proton irradiation," *Energy Environ. Sci.*, vol. 12, no. 5, pp. 1634–1647, 2019, doi: 10.1039/c9ee00077a.
- [60] F. Lang, O. Shargaieva, V. V. Brus, H. C. Neitzert, J. Rappich, and N. H. Nickel, "Influence of radiation on the properties and the stability of hybrid perovskites," *Adv. Mater.*, vol. 30, no. 3, pp. 1–22, 2018, doi: 10.1002/adma.201702905.
- [61] V. V. Brus *et al.*, "Defect Dynamics in Proton Irradiated CH<sub>3</sub>NH<sub>3</sub>PbI<sub>3</sub> Perovskite Solar Cells," *Adv. Electron. Mater.*, vol. 3, no. 2, 2017, doi: 10.1002/aelm.201600438.
- [62] J. Huang *et al.*, "Effects of Electron and Proton Radiation on Perovskite Solar Cells for Space Solar Power Application," *2017 IEEE 44th Photovolt. Spec. Conf. PVSC 2017*, pp. 1–6, 2017, doi: 10.1109/PVSC.2017.8366410.
- [63] S. Yang, Z. Xu, S. Xue, P. Kandlakunta, L. Cao, and J. Huang, "Organohalide Lead Perovskites: More Stable than Glass under Gamma-Ray Radiation," *Adv. Mater.*, vol. 31, no. 4, pp. 1–7, 2019, doi: 10.1002/adma.201805547.
- [64] A. G. Boldyreva *et al.*, "γ-Ray-induced degradation in the triple-cation perovskite solar cells," *J. Phys. Chem. Lett.*, vol. 10, no. 4, pp. 813–818, 2019, doi: 10.1021/acs.jpcclett.8b03222.
- [65] G. M. Paternò *et al.*, "Perovskite solar cell resilience to fast neutrons," *Sustain. Energy Fuels*, vol. 3, no. 10, pp. 2561–2566, 2019, doi: 10.1039/c9se00102f.
- [66] I. Cardinaletti *et al.*, "Organic and perovskite solar cells for space applications," *Sol. Energy Mater. Sol. Cells*, vol. 182, pp. 121–127, 2018, doi: 10.1016/j.solmat.2018.03.024.
- [67] Y. Tu, G. Xu, X. Yang, Y. Zhang, Z. Li, and R. Su, "Mixed-cation perovskite solar cells in space," *Sci. China Physics, Mech. Astron.*, vol. 62, no. 7, pp. 7–10, 2019.
- [68] W. S. Yang *et al.*, "High-performance photovoltaic perovskite layers fabricated through intramolecular exchange," *Science (80-. )*, vol. 348, no. 6240, pp. 1234–1237, 2015, doi: 10.1126/science.aaa9272.
- [69] N. J. Jeon, J. H. Noh, Y. C. Kim, W. S. Yang, S. Ryu, and S. Il Seok, "Solvent engineering for high performance inorganic organic hybrid perovskite solar cells," *Nat. Mater.*, vol. 13, no. September, pp. 897–903, 2014, doi: 10.1038/NMAT4014.
- [70] C. Hulubei *et al.*, "Antagonistic effects in structural design of sulfur-based polyimides as shielding layers for solar cells," *Sol. Energy Mater. Sol. Cells*, vol. 193, no. July 2018, pp. 219–230, 2019, doi: 10.1016/j.solmat.2019.01.018.

- [71] B. Hailegnaw, G. Adam, D. Wielend, J. D. Pedarnig, N. S. Sariciftci, and M. C. Scharber, "Acetylacetone Improves the Performance of Mixed Halide Perovskite Solar Cells," *J. Phys. Chem. C*, vol. 123, pp. 23807–23816, 2019, doi: 10.1021/acs.jpcc.9b05058.
- [72] B. Hailegnaw *et al.*, "Inverted (p-i-n) perovskite solar cells using a low temperature processed TiOx interlayer," *RSC Adv.*, pp. 24836–24846, 2018, doi: 10.1039/c8ra03993c.
- [73] L. Rakocevic *et al.*, "Reliable Performance Comparison of Perovskite Solar Cells Using Optimized Maximum Power Point Tracking," *Sol. RRL*, vol. 1800287, pp. 1–9, 2019, doi: 10.1002/solr.201800287.
- [74] R. Wang, M. Mujahid, Y. Duan, Z. K. Wang, J. Xue, and Y. Yang, "A Review of Perovskites Solar Cell Stability," *Adv. Funct. Mater.*, vol. 29, no. 47, pp. 1–25, 2019, doi: 10.1002/adfm.201808843.
- [75] G. Grancini *et al.*, "One-Year stable perovskite solar cells by 2D/3D interface engineering," *Nat. Commun.*, vol. 8, pp. 1–8, 2017, doi: 10.1038/ncomms15684.
- [76] W. Kong *et al.*, "Characterization of an abnormal photoluminescence behavior upon crystal-phase transition of perovskite CH<sub>3</sub>NH<sub>3</sub>PbI<sub>3</sub>," *Phys. Chem. Chem. Phys.*, vol. 17, no. 25, pp. 16405–16411, 2015, doi: 10.1039/c5cp02605a.
- [77] K. Wu *et al.*, "Temperature-dependent excitonic photoluminescence of hybrid organometal halide perovskite films," *Phys. Chem. Chem. Phys.*, vol. 16, no. 41, pp. 22476–22481, 2014, doi: 10.1039/c4cp03573a.
- [78] S. Hegedus and W. Shafarman, "Thin-Film Solar Cells: Device Measurements and Analysis," *Prog. Photovoltaics Res. Appl.*, vol. 176, pp. 155–176, 2004, doi: 10.1002/pip.518.
- [79] M. Jaysankar *et al.*, "Minimizing Voltage Loss in Wide-Bandgap Perovskites for Tandem Solar Cells," *ACS Energy Lett.*, vol. 4, no. 1, pp. 259–264, 2019, doi: 10.1021/acscenergylett.8b02179.
- [80] W. Tress, M. Yavari, K. Domanski, P. Yadav, B. Niesen, and P. Correa, "Interpretation and evolution of open-circuit voltage, recombination, ideality factor and subgap irreversible degradation of perovskite solar cells," *Energy Environ. Sci.*, vol. 11, pp. 151–165, 2018, doi: 10.1039/C7EE02415K.
- [81] H. Zhang, X. Qiao, Y. Shen, and M. Wang, "Effect of temperature on the efficiency of organometallic perovskite solar cells," *J. Energy Chem.*, vol. 24, no. 6, pp. 729–735, 2015, doi: 10.1016/j.jechem.2015.10.007.
- [82] B. Zhao *et al.*, "The application of Al<sub>2</sub>TiO<sub>5</sub> at the TiO<sub>2</sub>/perovskite interface to decrease carrier losses in solar cells," *J. Mater. Chem. A*, vol. 5, no. 7, pp. 3691–3698, 2017, doi: 10.1039/c6ta10468a.
- [83] N. K. Elumalai and A. Uddin, "Open circuit voltage of organic solar cells: An in-depth review," *Energy Environ. Sci.*, vol. 9, no. 2, pp. 391–410, 2016, doi: 10.1039/c5ee02871j.
- [84] O. Gunawan, T. K. Todorov, and D. B. Mitzi, "Loss mechanisms in hydrazine-processed Cu<sub>2</sub>ZnSn(Se,S) 4 solar cells," *Appl. Phys. Lett.*, vol. 97, no. 23, pp. 2008–2011, 2010, doi: 10.1063/1.3522884.
- [85] S. Shao *et al.*, "Efficient Perovskite Solar Cells over a Broad Temperature Window: The Role of the Charge Carrier Extraction," *Adv. Energy Mater.*, vol. 7, no. 22, 2017, doi: 10.1002/aenm.201701305.
- [86] A. D. Sheikh *et al.*, "Effects of High Temperature and Thermal Cycling on the Performance of Perovskite Solar Cells: Acceleration of Charge Recombination and Deterioration of Charge Extraction," *Appl. Mater. Interfaces*, 2017, doi: 10.1021/acsami.7b11250.
- [87] I. Mesquita, L. Andrade, and A. Mendes, "Temperature Impact on Perovskite Solar Cells Under Operation," *ChemSusChem*, pp. 2186–2194, 2019, doi: 10.1002/cssc.201802899.
- [88] R. Cheacharoen, N. Rolston, and D. Harwood, "Design and understanding of encapsulated perovskite solar

- cells to withstand temperature," *RSC Energy Environ. Sci.*, pp. 144–150, 2018, doi: 10.1039/c7ee02564e.
- [89] Y. Kim *et al.*, "Engineering interface structures between lead halide perovskite and copper phthalocyanine for efficient and stable perovskite solar cells," *RSC Energy Environ. Sci.*, pp. 2109–2116, 2017, doi: 10.1039/c7ee01931a.
- [90] F. Ruf, N. Giesbrecht, B. Rendenbach, A. Magin, and M. Hetterich, "Temperature-dependent studies of exciton binding energy and phase-transition suppression in ( Cs , FA , MA ) Pb ( I , Br ) 3 perovskites  
Temperature-dependent studies of exciton binding energy and phase-transition suppression in ( Cs , FA , MA ) Pb ( I , , " vol. 031113, 2019, doi: 10.1063/1.5083792.
- [91] P. P. Jenkins *et al.*, "Initial results from the second forward technology solar cell experiment," *Conf. Rec. IEEE Photovolt. Spec. Conf.*, pp. 1124–1127, 2010, doi: 10.1109/PVSC.2010.5614728.